

Review Article

Marc A. Verschuuren*, Mischa Megens, Yongfeng Ni, Hans van Sprang and Albert Polman

Large area nanoimprint by substrate conformal imprint lithography (SCIL)

DOI 10.1515/aot-2017-0022

Received March 14, 2017; accepted April 28, 2017

Abstract: Releasing the potential of advanced material properties by controlled structuring materials on sub-100-nm length scales for applications such as integrated circuits, nano-photonics, (bio-)sensors, lasers, optical security, etc. requires new technology to fabricate nano-patterns on large areas (from cm² to 200 mm up to display sizes) in a cost-effective manner. Conventional high-end optical lithography such as stepper/scanners is highly capital intensive and not flexible towards substrate types. Nanoimprint has had the potential for over 20 years to bring a cost-effective, flexible method for large area nano-patterning. Over the last 3–4 years, nanoimprint has made great progress towards volume production. The main accelerator has been the switch from rigid- to wafer-scale soft stamps and tool improvements for step and repeat patterning. In this paper, we discuss substrate conformal imprint lithography (SCIL), which combines nanometer resolution, low patterns distortion, and overlay alignment, traditionally reserved for rigid stamps, with the flexibility and robustness of soft stamps. This was made possible by a combination of a new soft stamp material, an inorganic resist, combined with an innovative imprint method. Finally, a volume production solution will be presented, which can pattern up to 60 wafers per hour.

Keywords: high volume manufacturing; nanoimprint; overlay alignment; PDMS; soft stamps; sol-gel resist.

*Corresponding author: **Marc A. Verschuuren**, Philips SCIL Nanoimprint Solutions, De Lismortel 31, 5612 AR, Eindhoven, The Netherlands, e-mail: marc.verschuuren@philips.com
Mischa Megens, Yongfeng Ni and Hans van Sprang: Philips Research, High Tech Campus 4, 5656AE, Eindhoven, The Netherlands
Albert Polman: AMOLF, Amsterdam, The Netherlands

www.degruyter.com/aot

© 2017 THOSS Media and De Gruyter

1 Introduction

Nanoimprinting is a versatile technique for fabricating nanostructures in which a master pattern is replicated via a stamping process, which uses physical contact to mold a liquid material in the inverse shape of the stamp, solidify the material, and remove the stamp [1–3]. Nanoimprint technology has the potential to economically deliver large areas of features with dimensions well below 1 μm. The markets for NIL with sub-100-nm resolution are versatile for applications such as vertical cavity surface emitting lasers (VCSELs) (lidar, miniature atomic clocks, pollution monitoring, optical communication), bar lasers (optical communication), solid-state lighting (LED substrates, light management, nano-LEDs), photovoltaics (light management, nano-wire based photovoltaic cells), sensors (DNA sequencing, glucose monitoring), security features (anti-counterfeit), and nano-photonics in general, especially in the field of meta-materials and meta-surfaces (invisibility cloak, flat lenses).

However, until recent years, nanoimprint has been confined to research and development to replicate large-area nanoscale resolution patterns due to intrinsic issues with this contact replication technique and lack of suitable material combinations. In the last 3–4 years, the request from industry for a nanoimprint-based volume production has shifted the nanoimprint community effort towards wafer-scale soft stamps.

Nanoimprint lithography techniques are generally classified by the stamp type used:

1. rigid (wafer scale)
2. rigid (step and repeat)
3. soft stamp (wafer scale)

Each method has advantages and disadvantages and specific applications for which it is most suitable. Historically, much effort has gone into the development of material and tooling for wafer-scale rigid stamp methods, as initially for this method, stamps (Si) and resist materials polymethylmethacrylate (PMMA), polystyrene (PS) were readily accessible and tooling is relatively low cost, as

only a heating stage and press is required. The method is well suited to replicate nano-patterns in thick (millimeter-scale) polymer sheets. However, the basic issues of bringing two rigid plates into contact within 10–100 nm, which is required to transfer imprinted patterns into subsequent layers/materials, prevailed. Further issues are as follows:

- Releasing two rigid plates in intimate contact requires high forces, which lead to shearing forces that can damage features on release [3, 4] (See Figure 1A).
- Achieving sub-100-nm overlay alignment on wafer scale is also challenging due to the thermal cycle and high pressure process [4].
- During release, the forces on the nano-patterns lead to degradation of the non-stick layer on the stamp [5–7].
- Air/gas inclusions in the features leading to non-filled patterns [8, 9]
- Fragile expensive stamps and damage due to particles [10]
- Damage and breakage of products

In order to pattern a whole wafer area without the high forces, the step and repeat method uses a small area fused with silica stamp and a low-viscosity UV curing resist (Figure 1A). Overlay alignment is achieved by positioning the stamp, while it is in contact with the resist. This makes the method suitable for IC applications, which also has extremely clean and flat substrates, which relax the sensitivity to particle contaminants. Disadvantages are as follows:

- Costly stamps
- Stamp degradation by release and particle contaminants [5–7]

- Air/gas inclusions in the features leading to non-filled patterns [11, 12]
- Limited application scope

The third method uses soft stamps and was initially developed to locally deposit a monolayer of material by contacting a chemical loaded silicone rubber stamp [13]. Wafer-scale silicone rubber (poly-dimethyl-siloxane, PDMS) stamps are replicated themselves from a master pattern (rigid, polymer, glass, etc.), and as they are flexible, these are easily released. Besides patterning monolayers, the stamp can also be used to imprint liquid resists. The flexibility of the PDMS stamps allows conformal contact on full wafer areas without application of external pressure (see Figure 1A, B). The method is applicable to applications such as nano-photonics (LEDs, lasers, meta-surfaces), (bio-)sensors, and more general applications that require nano- or micro-patterns on large areas. However, the softness of the stamp material leads to different issues:

- limited resolution due to unstable micro- and nano-patterns due to surface tension [14, 15],
- incompatibility with resist materials diffusing into the stamp [16–19], and
- in-plane pattern deformation limiting overlay performance [20, 21].

In this work, we will present a form of soft lithography that combines the advantages of rigid stamps (resolution, low pattern distortions) with the low-cost, wafer-scale patterning from soft stamps while achieving sub-10-nm feature resolution, sub-10-nm overlay alignment, a

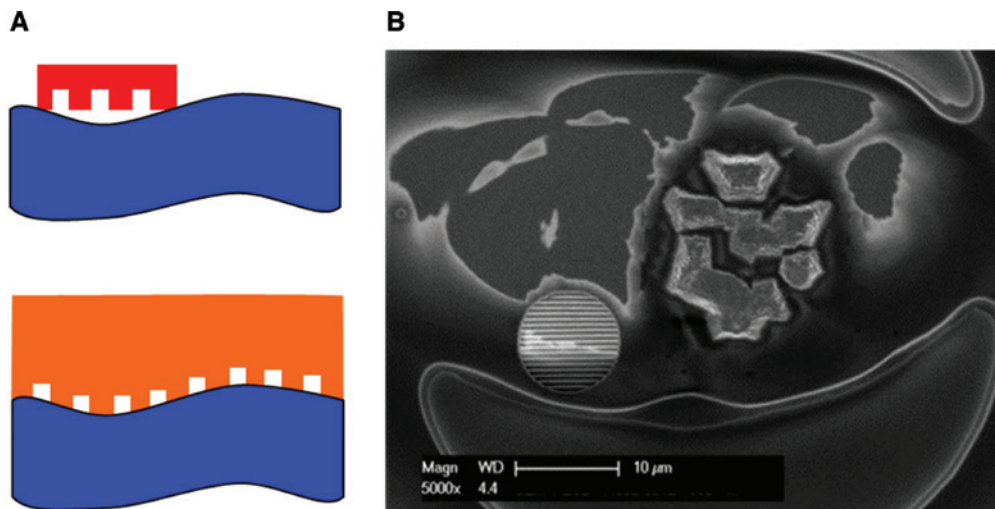


Figure 1: A small area stamp (top) will allow relatively intimate contact to be made, relaxing substrate flatness requirements. A rubber stamp follows the substrate on wafer scales. (A) The fundamental difference between a rigid stamp and a soft stamp in intimate contact with a substrate. (B) Typical defect on VCSEL laser substrates due to epitaxial growth defects. A soft stamp is not damaged by the defect.

functional hard mask resist, and long stamp lifetime. Substrate conformal imprint lithography (SCIL) has been used to fabricate polarization stable VCSEL lasers [22], (see Figure 1B) photonic crystal LEDs [23], three-dimensional (3D) photonic structures [24], and (nano-)patterned sapphire substrates (PSS) (LED substrates) [25] See Figure 2. Additionally, it was used for large-area device fabrication of nano-spectrometers [26], large-area plasmonics for photovoltaics [27, 28], solid-state lighting [29, 30], nano-hole arrays [31], nano-wire growth templates [32, 33], and novel nano- and micro- magnetic configurations [34, 35].

2 High-resolution soft stamps

Although isolated nanometer-sized features have been replicated using PDMS and higher hardness PDMS formulations [36], these are still insolated patterns. Replicating dense sub-100-nm features such as gratings pose more

challenges and lead to collapsing patterns, as shown in Figure 3. PDMS has been the material of choice for the soft-lithography field, although other material systems have been investigated. Notably, perfluoro-polyethers (PFPE) form a rubber-like material after cross-linking with the aid of a UV radical initiator and are able to replicate dense nano-patterns as well. However, PFPE does not possess real rubber-like properties (Poisson ratio 0.5) and exhibits viscous elastic flow, which will influence/degrade (nano-) patterns, especially due to the applied stresses from imprinting and release of the stamp [16].

Increasing the Young's modulus of the stamp will prevent collapse of high density patterns; however, by increasing the Young's modulus, the issues from rigid stamps arise again [37]. However, up to a modulus of ~ 100 MPa, the stamp material is able to support non-collapsing dense nano-patterns but still make conformal contact over wafer-scale areas, provided the high-modulus PDMS material is a thin layer (less than $100 \mu\text{m}$).

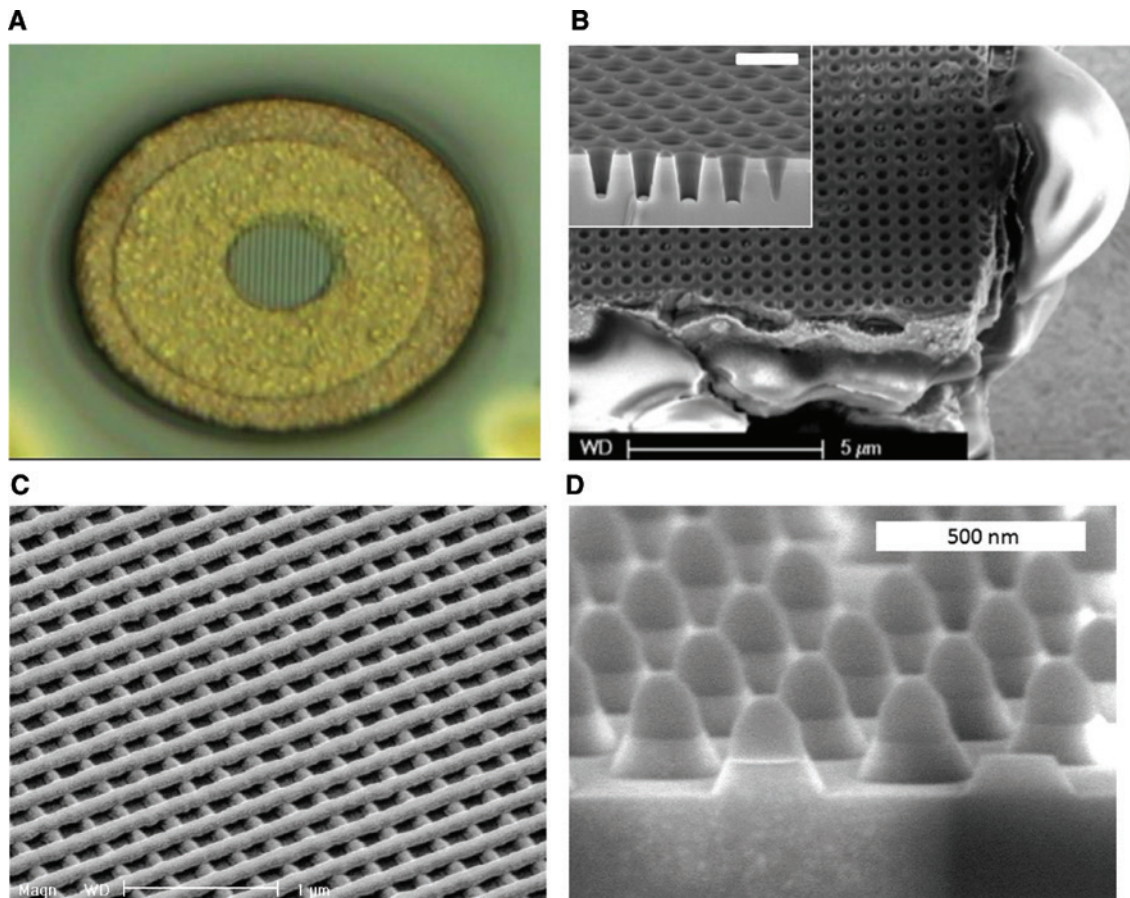


Figure 2: Application examples for soft-stamp NIL. (A) Optical photograph of VCSEL p-contact and output aperture in the center, which contains the nano-grating (550-nm period). (B) SEM photograph of a GaN LED surface with imprinted and etched photonic crystal, inset shows SEM cross-section of etched photonic crystal in GaN. (C) SEM of four-layer stack of silica gratings after burn-out of sacrificial polymer. (D) SEM cross-section of nano-PSS pattern in sapphire, sol-gel etch mask is still present.

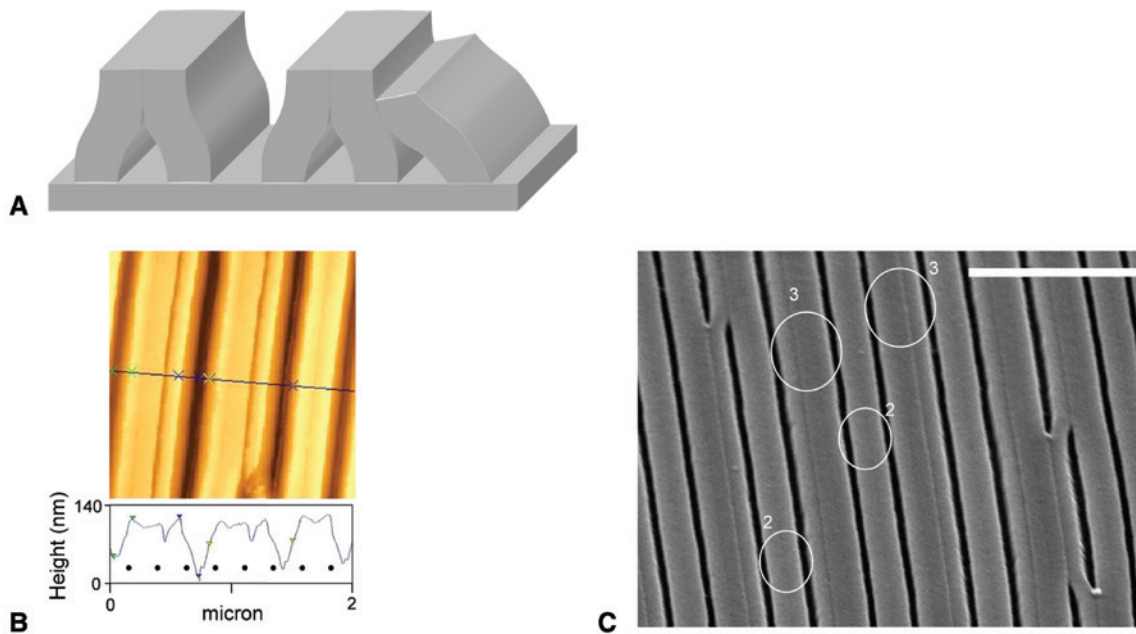


Figure 3: Soft-stamp deformations due to surface tension. (A) Schematic of paired grating features, (B) AFM data: 2D height profile and line scan perpendicular to the grating lines. The dot pattern schematically shows a pitch of 240 nm. (C) SEM image of H-PDMS grating of 115-nm high, 80-nm-wide lines on a pitch of 240 nm. The grating has collapsed and two or three individual lines stick together (indicated by the white circles). The scale bar in (C) is 2 μm .

To achieve wafer-scale conformal contact using low pressure, SCIL uses a composite stamp composed of two rubber layers on a thin glass support, see Figure 4 [15, 38, 39]. The nano-patterns are molded in a thin layer made from a stiff silicone rubber, X-PDMS supplied by Philips

SCIL Nanoimprint Solutions (Eindhoven, The Netherlands), which can attain a modulus up to 80 MPa and allows for accurate replication of nanometer-sized structures. This layer is grafted on a thin glass plate by a low modulus silicone rubber (Dow Corning Corporation,

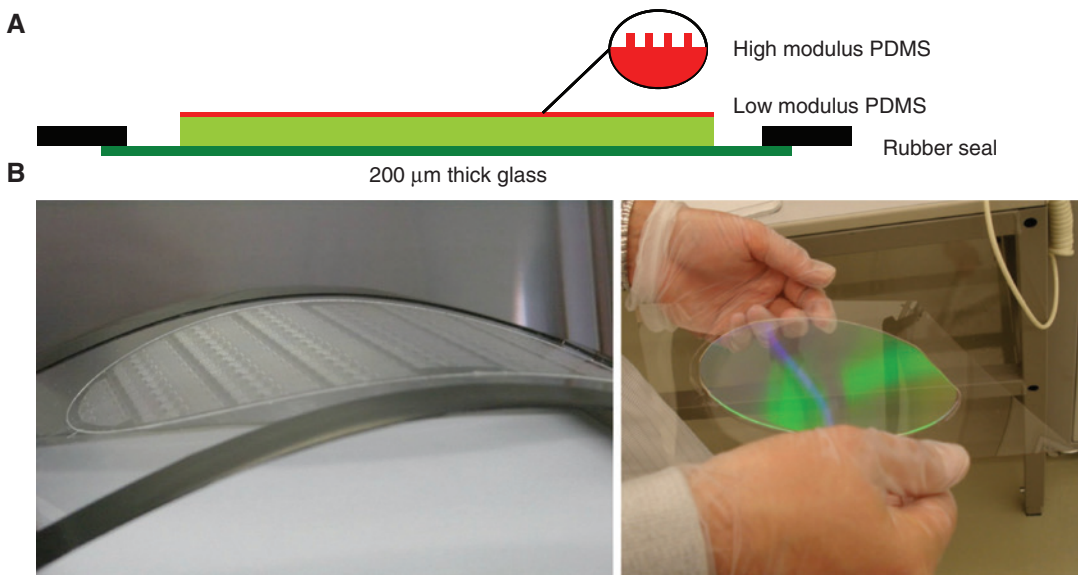


Figure 4: Tri-layer SCIL stamp build-up. (A) Schematic of a SCIL composite stamp consisting of a thin glass carrier plate on which a two-layer silicone rubber stamp is attached. The top PDMS layer consists of high-modulus X-PDMS and contains the patterns. The low modulus of the bottom PDMS layer helps to make conformal contact during imprinting, (B) Photographs of SCIL stamps, showing the flexibility in the out-of-plane direction by bending the stamp. In the right picture, interference colors can be seen which result from a pillar pattern with a pitch of 513 nm in the X-PDMS.

Auburn, Michigan, USA, Sylgard 184). The thin glass is flexible in the out-of-plane direction, which allows conformal contact to be made over wafer-scale areas, but stiff in plane, which prevents pattern placement distortions. The modulus of the X-PDMS in a three-layer stamp can reach up to 100 MPa but still make conformal contact as the whole stamp is flexible on varying length scales (micrometer to centimeter scale). The stamp can be removed from the master in a peeling-like manner with low force, while the in-plate stiffness of the glass sheet avoids pattern distortions. SCIL combines the resolution and accuracy of rigid stamps with the flexibility of soft stamp methods.

A typical SCIL stamp consists of a square glass sheet with a thickness of 200 μm . On this glass, $\sim 0.5\text{-mm}$ -thick PDMS rubber stamp is grafted. This geometry allows bending of the stamp in the out-of-plane direction to conform to surface roughness and substrate bow, while pattern distortions are minimized due to the in-plane stiffness of the glass plate.

The X-PDMS rubbers are too stiff to make the stamp entirely from X-PDMS, as this would compromise the conformal contact. The high modulus is also a disadvantage during imprinting when large particles are present and the ‘bulk’ rubber has to deform to accommodate the deformation. Therefore, the rubber is built up from a thin layer of high-modulus X-PDMS (which contains the patterns) and bulk layer of soft and tough commercial PDMS [15, 37].

To produce an SCIL stamp, the master containing the patterns is first prepared. A 10–50- μm -thick layer of X-PDMS is spin coated over the master and pre-cured for 5–10 min at 50°C. After the pre-cure, the X-PDMS is tacky and a second, intermediate layer is applied. These two layers are subsequently cured at 90°C until the desired Young’s modulus is reached. Table 1 shows the Young’s modulus of the X-PDMS as measured by AFM pico-indentation as function of the curing time and temperature. The maximum indentation was kept below 1 μm as to stay below 10% of the X-PDMS layer thickness and thus only measure the X-PDMS layer and not the underlying intermediate- and soft-PDMS layers.

Table 1: Youngs’ modulus obtained by pico-indentation of SCIL composite PDMS stamps.

PDMS type	Curing time	Temperature (°C)	Young’s modulus (MPa)
X-PDMS	30 min + 2 h	70 + 50	36
X-PDMS	1 day	70	48
X-PDMS	1 day	90	57
X-PDMS	5 days	90	85
H-PDMS	4 days	50	13
Sylgard 184	4 days	50	3.5–4

After the X-PDMS has reached the desired modulus such that the patterns in the stamp are mechanically robust, the final SCIL stamp is made. A SussMicroTecstamp replication tool is used to fabricate the SCIL composite stamps without air inclusions and ensure homogeneous heating during curing of the soft-PDMS. It consists of two parallel vacuum chucks that are heated and where the distance between the chucks is controlled by three micrometer spindles. The X-PDMS coated master is placed on the bottom vacuum chuck. Next, Sylgard 184 soft-PDMS is mixed and de-gassed and a precise amount is poured on the X-PDMS coated master. Subsequently, the top vacuum chuck, which holds the thin glass plate, is lowered, which causes squeezing out of the commercial PDMS over the master. The final thickness is controlled by the three spindles. As the soft PDMS cures, it bonds to the X-PDMS layer and the glass. After release from the tool, the composite stamp can be carefully peeled from the master. Finally, a rubber seal is glued on the edge of the glass. Figure 4A shows the schematic stamp layout, and Figure 4B shows photographs of two SCIL stamps demonstrating the out-of-plane flexibility and a large (150-mm diameter) stamp area, which displays interference colors due to the patterns in the rubber.

Wafer-scale imprints are made using the SCIL setup, which uses local pneumatic pressure to stepwise form full contact on a wafer coated with a thin liquid resist layer silica sol-gel based (Philips SCIL Nanoimprint Solutions), Ormocer types (AMO GmbH [25, 40], Aachen, Germany, and Micro Resist Technology GmbH, Berlin, Germany) and fully organic resists (DELO Industrial Adhesives, Windach, Germany [19] and Micro Resist Technology). After the resist has hardened, the stamp is released in a smooth peeling-like action by a step-wise application of vacuum. The key difference is that the slight pneumatic over-pressure is only used to release the stamp from the groove plate in a controlled manner, and once the stamp makes contact in the liquid resist, the driving force is actually the capillary force, which pulls the stamp into the resist due the capillary action. This makes for a smooth, continuous advance of the substrate-resist-stamp contact line, which pushes the ambient air out in front of the stamp. See SCIL process cycle in Figure 5.

Provided the resist has a contact angle on the PDMS stamp of less than 90°, there will be a capillary force that pulls the stamp into the liquid resist. This capillary force also assists in filling up features in the stamp with resist. This creates a local overpressure on any air that is trapped in a stamp feature and aids in the fact that air quickly diffuses into the PDMS stamp [41]. On release of the stamp, the gasses can diffuse out again.

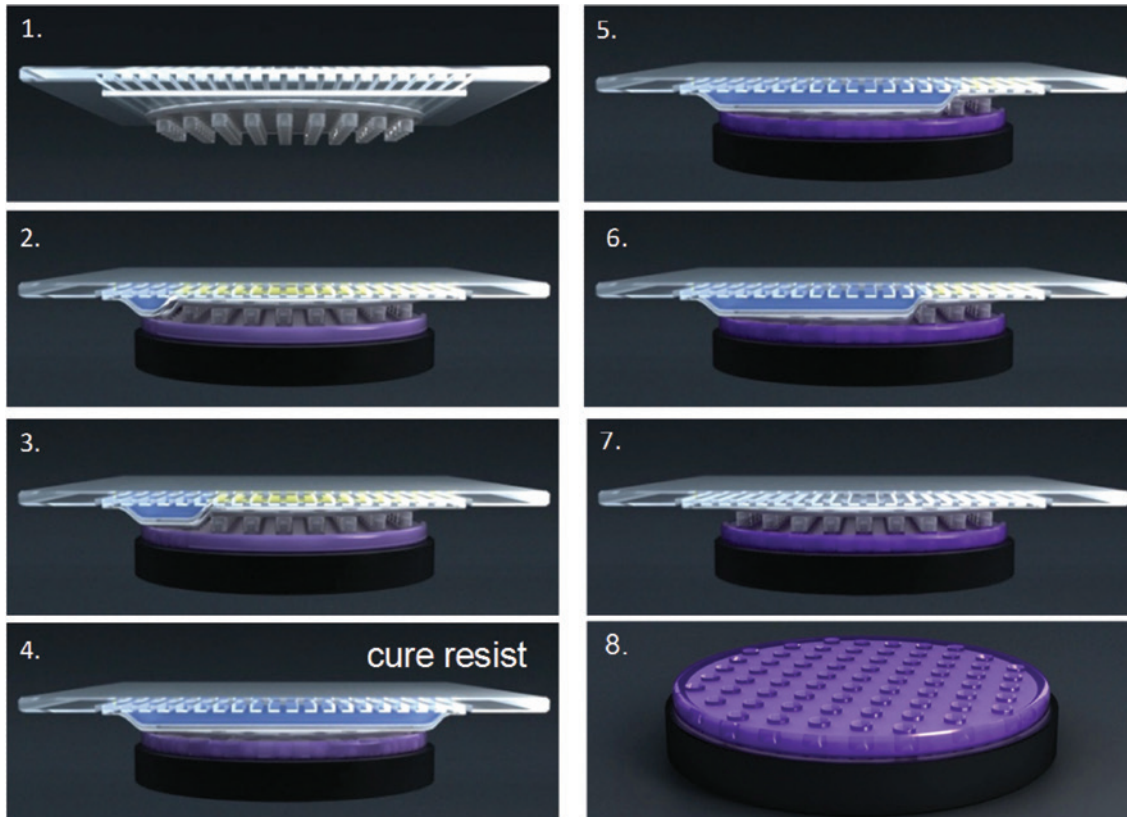


Figure 5: SCIL imprint and release sequence. (1) Stamp is held by vacuum on the SCIL groove plate actuator. (2) A liquid resist coated wafer is loaded and brought to within $\sim 100\text{-}\mu\text{m}$ distance of the stamp. Next, a slight overpressure is sequentially applied to the grooves, which makes the stamp bulge out and contact the resist. (3) Once contact is made in the resist, it is actually the capillary force that pulls in the resist and pulls the stamp in. The remaining grooves are pressured, which leads to a controlled release of the stamp. (4) The moment the whole stamp is in contact with the resist on the wafer, the resist is cured, either by UV or thermally. (5–6) After the resist has transformed from liquid (to gel) into solid, the grooves are sequentially switched back to vacuum, which pulls the stamp on the groove plate. This will peel the stamp from the resist in an almost vertical motion. (7) The sequential release process continues until all the grooves are at vacuum again and the stamp is back at the initial position. (8) The distance between stamp and imprinted wafer is increased and the imprinted product is unloaded.

The SCIL technology has multiple advantages over methods that use rigid stamps:

- Conformal contact can be made over large areas without the use of a high pressure as the flexible stamp follows the substrate curvature.
- Micro-scale air inclusions and partially filled features are avoided as silicone rubber has a high permeability for solvents and gasses, which allows trapped air to diffuse into the stamp [42].
- Particle contaminants are less problematic as the rubber can locally deform around a particle, avoiding damage to the stamp or substrate.
- Release of a rubber stamp from a rigid imprinted pattern is aided by the fact that the rubber temporarily deforms on release. This avoids damage to features in the resist or stamp and enables the replication of features with a high aspect ratio, in contrast to (UV-)

NIL in which the aspect ratio is often limited to below one [43].

- PDMS has an inherently low surface energy and is chemically non-reactive, and therefore, an anti-sticking layer is not needed.

Deformation of the stamp due to a particle contaminant is mostly dissipated in the soft intermediate PDMS layer. This localizes the deformation to the PDMS in the direct surrounding of the particle contaminant and ensures that the remainder of the area is imprinted without deformations. Figure 6 shows SEM images of SCIL imprints in sol-gel resist over particles with a height up to 10 times the resist layer thickness. As can be seen, the stamp imprints the patterns on and over the particle and the local deformation of the rubber stamp is clearly shown. Only a small distance away from the defect, the pattern continues

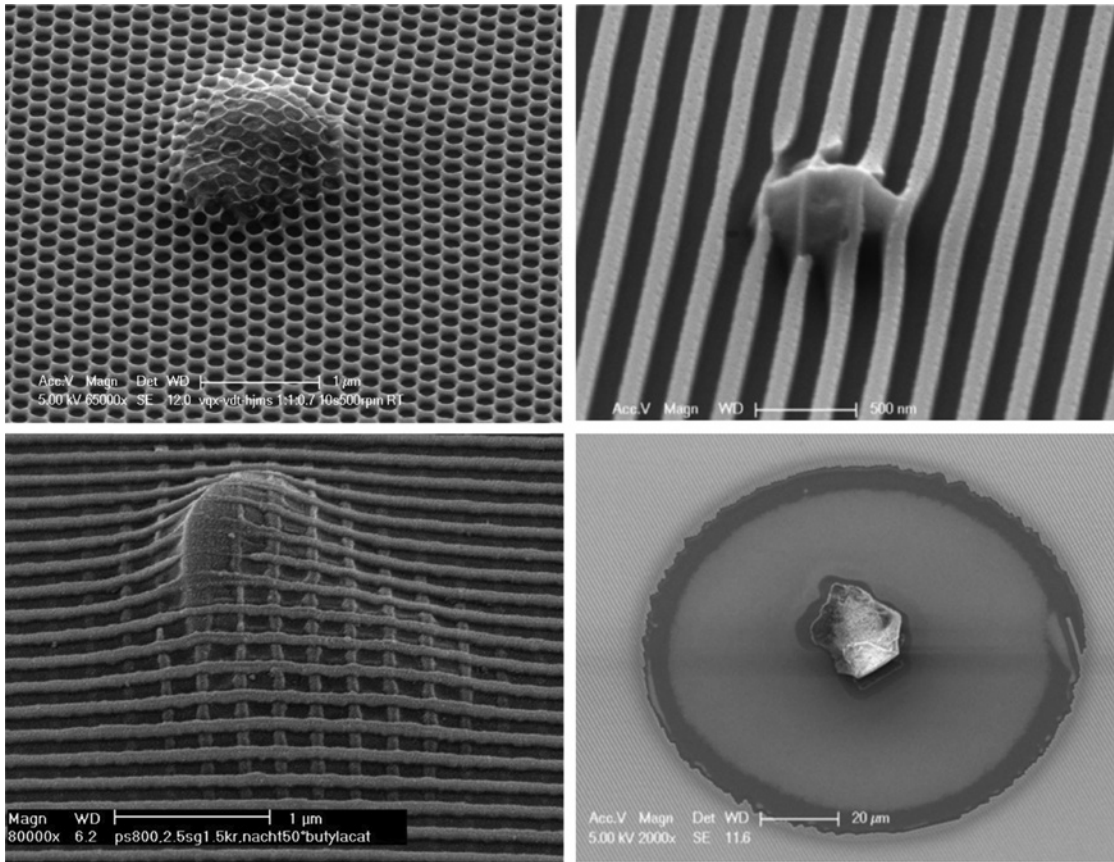


Figure 6: SEM images of sol-gel patterns made using SCIL on substrates with particle contaminants. Due to the softness of the stamp, the patterns are imprinted over particles, while the surrounding pattern is undisturbed.

without distortion. The bottom right picture shows an imprint over a particle which is $\sim 20 \mu\text{m}$ in height, which is too large to be fully dissipated in the rubber. This leads to an exclusion area of $\sim 100\text{-}\mu\text{m}$ diameter around the particle where no patterns are imprinted. When using a rigid stamp, these types of particles would cause damage to the stamp and/or substrate, potentially generating additional particles.

3 Nano-patterning using silica sol-gel based imprint resist

An essential advantage of PDMS stamps is that they can be used to pattern fully inorganic material systems. Philips developed a novel inorganic silica forming imprint resist based on the sol-gel route [22, 24, 37]. Philips delivers silica sol-gel based resist that cures without the need for UV radiation with optimized curing time for sol-gel resist V7 of less than 1 min at room temperature and allows direct patterning of silicon oxide

glass with nanometer resolution. The cured material can be directly used as hard mask in RIE processes to transfer patterns into an underlying layer with high fidelity. Furthermore, due to the light and temperature stability of imprinted silica, it can directly be used in (optical) applications. Figure 7 shows examples of SCIL imprinted sol-gel patterns, which demonstrate the high resolution and robustness of the technique using X-PDMS composite SCIL stamps. Figure 7A shows a grating with a pitch of 60 nm, with 25–30-nm wide grating lines. Figure 7B shows a hole-array with a pitch of 50 nm and 20–30-nm diameter holes. Clearly, the increased modulus of the X-PDMS results in features that are more stable against collapse (compared to, e.g. Figure 3) and enables the replication of dense patterns with dimensions as small as 25 nm and a pitch of 50 nm. This work proves that PDMS stamps are able to replicate high aspect ratio sub-25-nm patterns (Figure 7C) with all the advantages of soft stamps. The replicated patterns will convert to 100% dense fused silica at a temperatures of 850°C ; Figure 7D shows that the nanogratings retain their shape even after a 1000°C anneal.

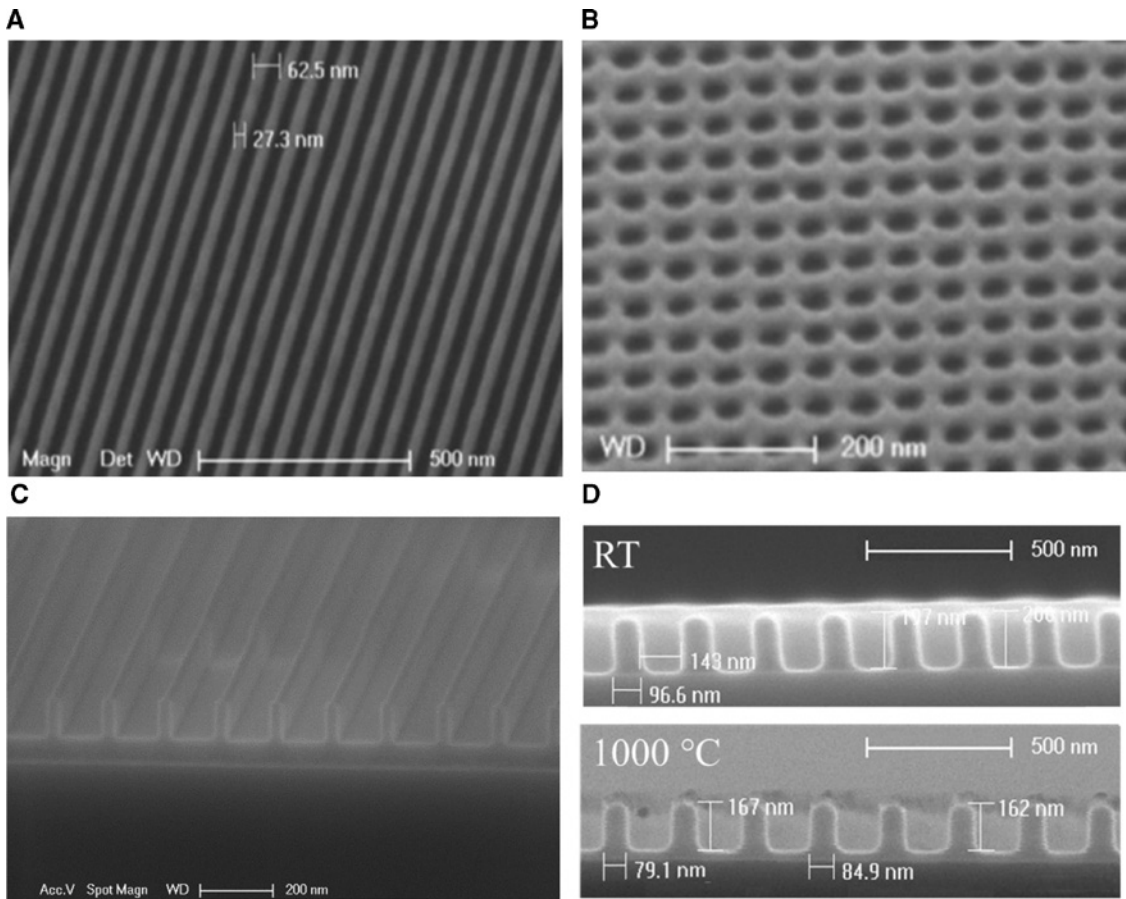


Figure 7: SEM images taken under an angle of 35° of a sol-gel layer patterned by X-PDMS stamps. (A) 60-nm pitch grating lines. (B) Square array of holes with 50-nm pitch. (C) 100-nm high, 25-nm wide, 150-nm period grating. (D) Cross-section of sol-gel gratings after replication at room temperature and anneal at 1000°C .

We believe that these dimensions are not the limit of the X-PDMS rubber system for dense patterns. In fact, the resolution of e-beam resist used to fabricate the master is limiting the production of dense regular patterns with a smaller pitch. The resolution limit of our X-PDMS material is determined not only by the geometrical stability of patterns but also by the ability of the rubber material to mold to a certain shape and hold this shape. Figure 8A shows SEM images, taken under an angle of 30° , of a master made by e-beam lithography and etching of quartz. It contains ~ 30 -nm diameter pillars on a pitch of 50 nm in square and hexagonal lattices. In a separate area, arrays are composed of features where during the e-beam process, two dots are written next to each other. During subsequent etching, these two closely spaced structures are transferred in the quartz as two separate dots, leaving a narrow gap of less than 10 nm, indicated by the circle in Figure 8A. This master pattern was replicated in sol-gel using an X-PDMS stamp. Figure 8B shows SEM images taken under an angle of 30° of the imprinted sol-gel patterns. As can be seen, the rubber is capable of reproducibly patterning 6-nm

gaps between arrays of sol-gel pillars. This indicates the potential of our material system to reproduce dense patterns on length scales below 10 nm.

3.1 Soft stamp imprint lifetime

For a contact lithography method, the stamp lifetime is of utmost importance. Especially for volume production, it is desired that a stamp is able to replicate the desired patterns without defects, preferentially indefinitely. There can be two main causes that lead to stamp degradation:

1. physical change to the stamp due to mechanical action
2. chemical modification of the stamp due to the interaction with the resist

As from 2008, VCSELs are produced using SCIL, which allowed us to test both degradation mechanisms [22]. The GaAs wafers with the full laser stack have many defects due to the epitaxial growth of many layers, where

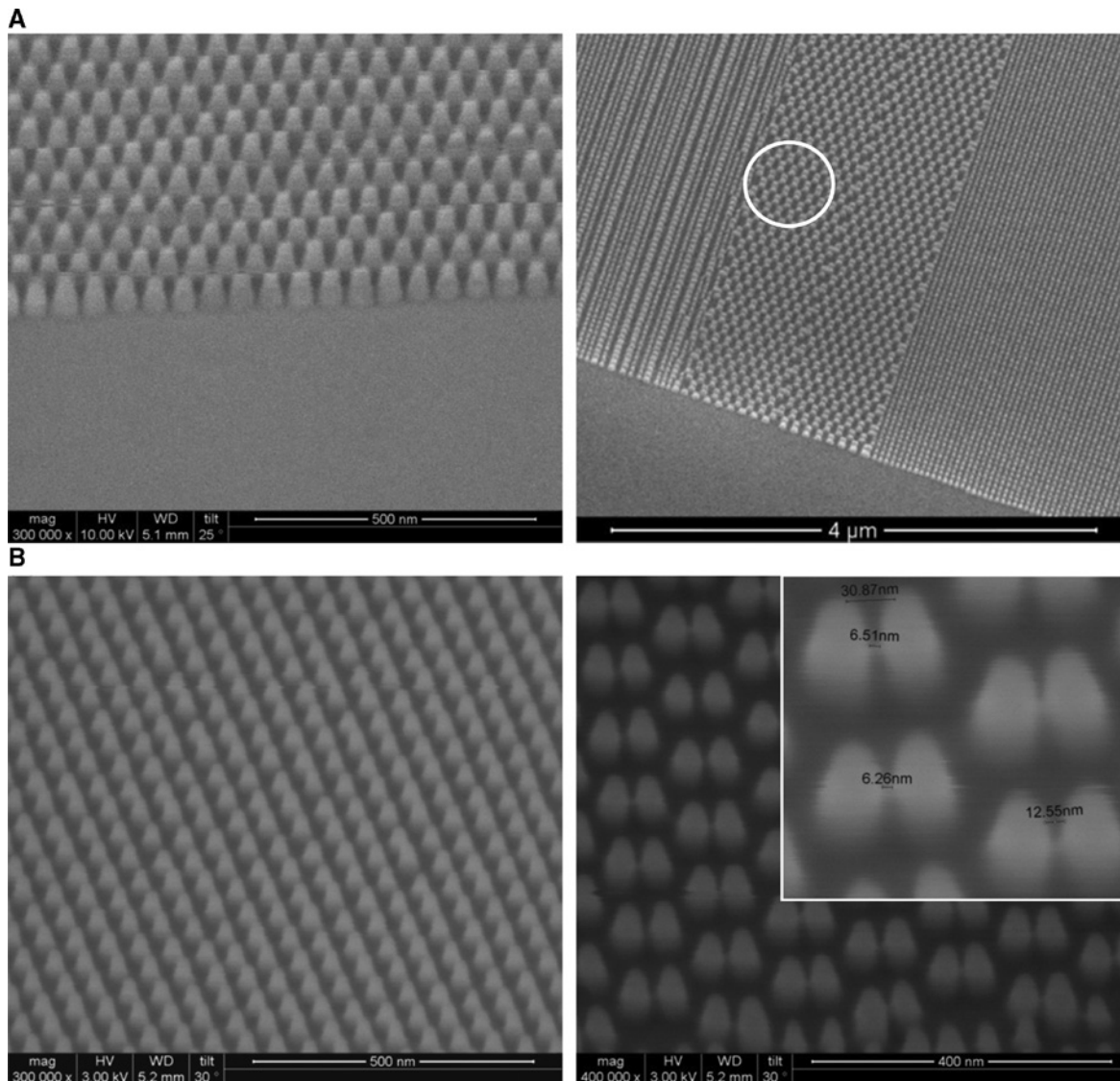


Figure 8: Comparison between the master and SCIL replicated patterns. (A) Quartz master pattern containing ~30-nm diameter pillars on a pitch of 50 nm and pillars spaced on a pitch of 30 nm, (B) sol-gel replica of the master patterns shown in (A).

around crystal defects macroscopic defects arise. See Figure 9, which shows the nano-gratings next to growth defects. Each imprint stamp thus experiences severe local distortions.

During VCSEL production, a single stamp was used for more than 600 imprints on 3" GaAs/VCSEL stack wafers. Each wafer was checked after imprinting and the residual layer etch by AFM. The height data are shown in Figure 10. All wafers showed high-quality patterns from which VCSEL lasers were produced. Comparing the yield of wafers with gratings produced by e-beam patterning and SCIL, we could conclude that the yield of SCIL was stable and equal or higher to e-beam patterning. This proves the point that stamps are not damaged due to particles/defects and are self-cleaning. Otherwise, the VCSEL

yield would have decreased with increasing number of imprints.

The resist/stamp interaction will influence the stamp lifetime, which was demonstrated for organic resists [17] and UV-assisted curing sol-gel resists [18]. From the VCSEL data, we conclude that when thermally curing sol-gel resist is used, we do not observe stamp degradation caused by chemical interactions of the sol-gel resist with the X-PDMS stamp material for at least 600 imprints.

4 Overlay alignment using SCIL

There are many applications that only require a single layer of nano-patterns. But for more advanced applications

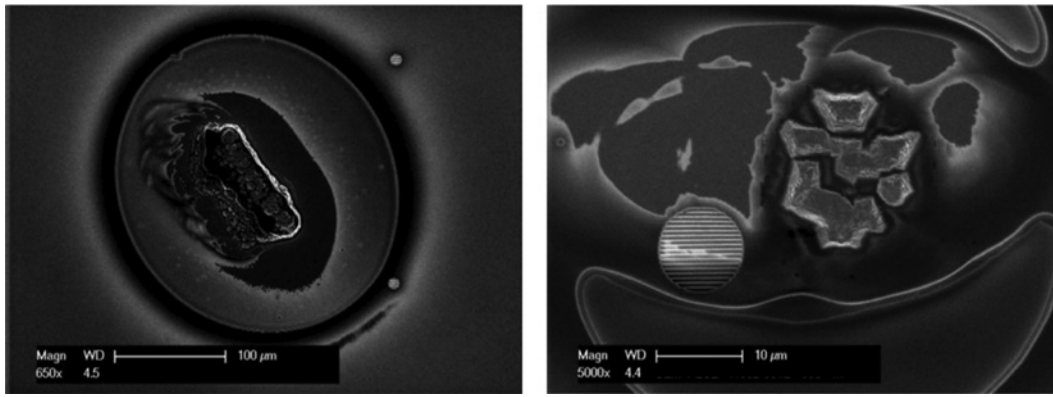


Figure 9: SEM images of SCIL imprinted nano-gratings in and around growth defects. The period is 550 nm, and line widths are 150 nm.

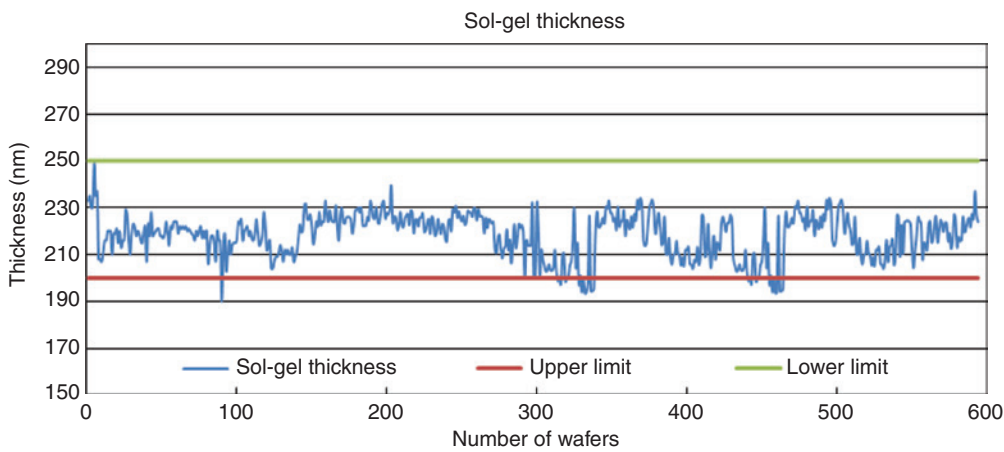


Figure 10: AFM height images of nano-gratings on GaAs after Cf₄/N₂ RIE break-through etch, replicated from the same SCIL stamp. The height variations are due to process variations during the RIE step. All wafers exhibited highly defined gratings, which could be used to transfer the nano-gratings into GaAs.

such as IC, complex sensors, MEMS and NEMS devices, there is a need to align several layers with respect to each other. Step and repeat imprint methods have focused from the beginning on overlay alignment and as these methods use a relatively small stamp in contact with the resist to align patterns to the wafer [10].

Alignment marker patterns can be used to determine the absolute or relative position between a stamp

and substrate and to detect pattern deformations. To provide absolute alignment down to ~1 μm, box-in-box type of alignment markers is used. These consist of a 50-μm-wide cross, which is located on the stamp (molded from a first master). The corresponding box, an area with a gap width of 70 μm in the form of a cross, is formed by imprinting sol-gel on a substrate (stamp molded from second master) (see Figure 11). The cross

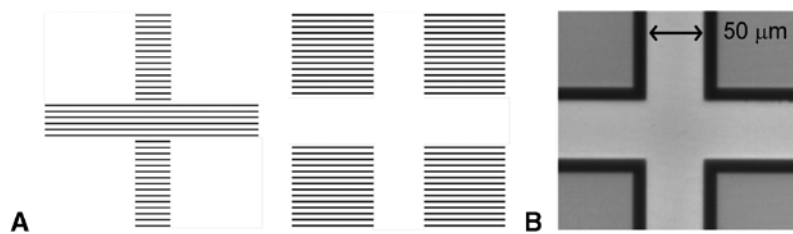


Figure 11: Box-in-box alignment marker layout. (A) Schematic of the cross (left) and box (right) marker, which are defined by gratings. (B) CCD image of a box-in-box alignment marker when the stamp (cross) is in contact with the substrate (box).

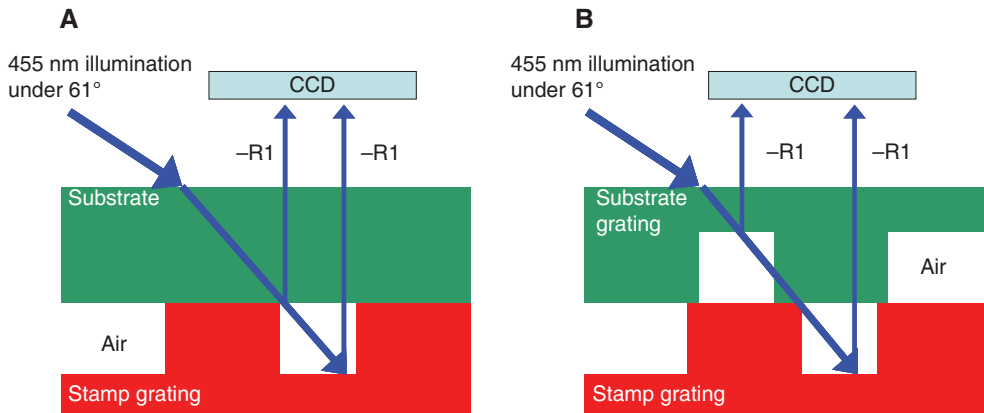


Figure 12: High contrast alignment marker illumination and detection scheme. (A) Schematic cross-section of the 580-nm pitch gratings used to generate high contrast alignment markers. (B) Schematic cross-section of the 580-nm pitch gratings used to generate Moiré patterns. Both gratings have a depth of 90 nm and a fill fraction of two-thirds.

and box patterns are composed of gratings with a pitch of 580 nm, see Figure 11A.

When illuminated with 450-nm light from a LED under an angle of 61° to the substrate normal, the first reflection order exits perpendicular to the substrate, see Figure 12A. The patterns are viewed using a long working distance objective coupled to a CCD camera. A picture of an aligned box-in-box marker in contact is shown in Figure 11B. The small difference in the brightness of the box and cross patterns is attributed to a small difference in fill fraction or refractive index between the two gratings (PDMS vs. sol-gel). The high contrast observed between grating and non-grating area enables accurate alignment of the two patterns.

4.1 The variation in magnification error between two stamps

The box-in-box alignment patterns can also be used to determine the difference in magnification error (defined as relative difference between master and stamp pattern) between two stamps. Magnification errors are predominantly caused by small variations in thermal cycles during stamp fabrication and a difference between the thermal expansion coefficients of master and stamp. If two stamps have been prepared at a different absolute temperature, the mismatch between the thermal expansion coefficient of master and glass back plate will produce a magnification error between the two stamps.

By comparing the alignments of two sets of box-in-box alignment markers spaced over a large distance, the magnification error can be determined. To make this comparison, a stamp is used to imprint the box pattern on a substrate. A second stamp with the corresponding cross is

then brought into contact to form the box-in-box pattern. The box-in-box markers are positioned 70 mm from each other. By simultaneously aligning the two markers, the distance between the middle cross on the substrate and the edge of the outer cross on the stamp is minimized. Figure 13 shows the aligned left and right stamp and substrate markers while in contact.

Computer pattern recognition was used to measure the distances between the cross and the box in both directions where the width of the middle cross was used for calibration. The distances were found to be all equal within the measurement accuracy of $\pm 0.25 \mu\text{m}$. This is much larger than the maximum position error of the e-beam generator ($\pm 25 \text{ nm}$), which was used to produce the two master patterns. The maximum magnification error between the two stamps is therefore $2 \times 0.25 \mu\text{m}$ over 70 mm, or 7 ppm. The measured magnification error of 7 ppm is the upper value due to the uncertainty in the optical measurement of the position of the crosses in the alignment markers. These values agree with the values found by Fader et al. in

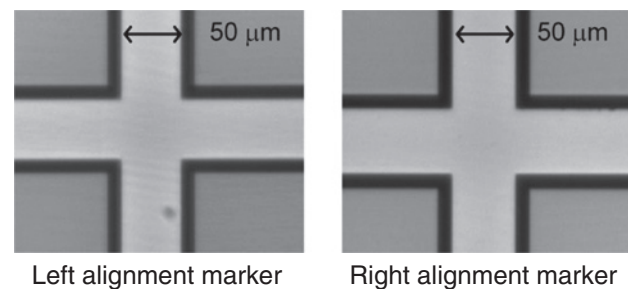


Figure 13: Two box-in-box type alignment markers in contact. The middle cross is 50- μm wide, and the space between the squares is 70 μm . The distance between the left and right marker on the wafer is 70 mm.

a different study where SCIL was used to imprint 200-mm wafers, and the position accuracy was measured over the wafer [44, 45].

4.2 Design of Moiré interference alignment markers and *in situ* pattern deformation characterization

Moiré interference techniques enable the detection of movements down to the nanometer level. Here, a Moiré pattern is formed by a grating on a substrate in contact with a grating in a stamp. This can result in light and dark patterns due to constructive or destructive interference of light in the two gratings [46]. To use Moiré patterns in the SCIL setup, the optical design depicted in Figure 12B was developed. The grating base period is 580 nm with a depth of 80–90 nm. The gratings are illuminated while in contact with 450-nm light from a LED under an angle of 61° to the substrate normal. Light from the first reflection orders of the top and bottom gratings interferes and forms a Moiré pattern, which is recorded using a CCD camera.

To control the period of the Moiré fringes, a Vernier Moiré technique was used in which two gratings of slightly different periods are in contact. To do so, two masters with corresponding grating patterns were produced by e-beam lithography and two SCIL stamps were molded from these masters. Using the SCIL setup, the patterns in the first stamp are imprinted in sol-gel resist on thoroughly cleaned AF32 glass substrates. The second stamp, which contains the corresponding grating, is then loaded in the SCIL setup and brought into contact with the first

imprinted gratings. In the experiments, using gratings with a fill fraction of ~ 0.5 , we noticed that the contrast of the Moiré patterns changed over time. We found that this is caused by grating lines that do not stay on top of each other as shown in Figure 12B but would actually sag between each other and interpenetrate. This changes the interference condition and thus the contrast of the Moiré pattern. By changing the grating duty cycle to two-thirds, we found that the Moiré patterns do not change contrast over a timescale of several days.

To determine absolute position errors using Moiré fringes, the absolute placement of the gratings has to be known to at least within half the grating pitch. This is due to the repetitive nature of the Moiré interference after one grating period. To enable absolute alignment down to nanometer accuracy, a method is needed that can detect absolute position changes from sub-millimeter to nanometer scale. Our design uses Moiré patterns with three length scales, which are subsequently aligned, starting with the coarse pattern.

Using the box-in-box alignment markers and the SCIL setup, the stamp and the substrate that contain the imprinted markers were aligned to within $1\ \mu\text{m}$. Figure 14 shows successive CDD images of a Moiré alignment marker pattern as the stamp is brought in contact with the substrate. The area over which a Moiré pattern is formed is $8 \times 6\ \text{mm}$. In Figure 14A, the stamp is in close proximity but not in contact; in (B), the stamp is partly in contact (arrow indicates the position of the contact front); the contact has advanced by 2.5 mm in (C); and in (D), full contact is established. In Figure 14D, from left to right, three different Moiré patterns are observed

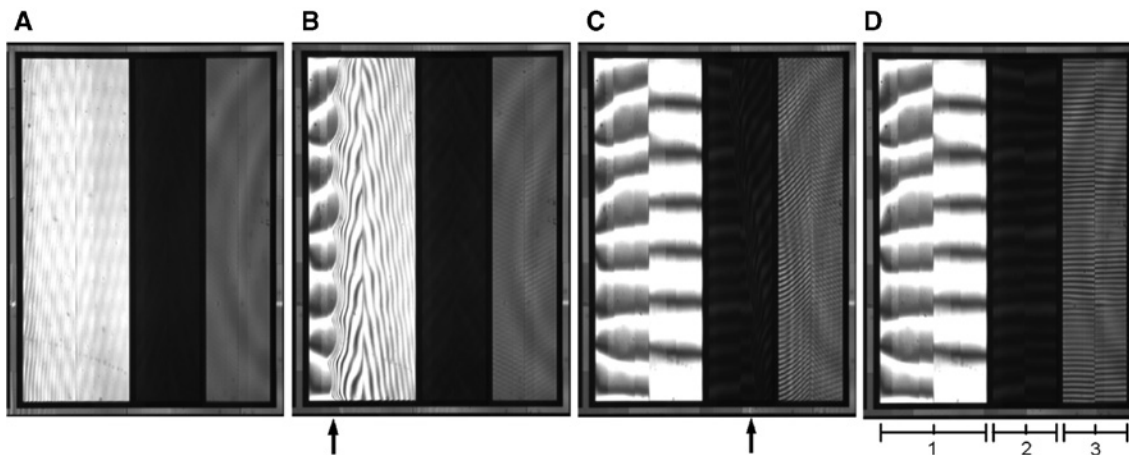


Figure 14: Three distinct pairs of Moiré patterns are formed as two grating sets are brought into contact using the SCIL setup, the contact line advancing 2.5 mm each time. (A) The stamp is in close proximity; (B–D) stamp in contact; in (B) and (C), the contact line is indicated by arrows; in (D), the stamp is in full contact. The numbered sections in (D) refer to grating pitches of (1) 580/580.3 nm, (2) 2317/2320 nm, (3) 10.000/10.050 μm .

(indicated as 1, 2, 3), which correspond to grating pitch combinations of 580/580.3 nm, 2317/2320 nm, 10.000/10.050 μm , respectively. These three Vernier gratings are used in pairs; for each pair, the left part of the pair has the shortest pitch located on the substrate and the right part has the shortest pitch located on the stamp. This design has the following advantages that, when the patterns are moved perpendicular to the grating direction in a pair, the left and right Moiré fringes move in opposite directions. This doubles the resolution per pixel as not the absolute shift of a Moiré fringe is measured but the relative shift between two Moiré fringes. The patterns are designed such that, for absolute alignment, all the fringes have to line up, as shown in Figure 14D. This pattern also helps to optimize the alignment procedure; if the previous alignment step accuracy is better than half the grating pitch of the next Moiré grating set, the fringes that have the smallest offset need to be aligned next.

The following patterns and features are observed in the Moiré patterns of Figure 14D. The 580/580.3-nm Moiré pattern has a high contrast and shows the predicted eight fringes. The 2317/2320-nm Moiré pattern shows a repeating pattern of three dim lines and a brighter fourth line. This can be explained as the 2317/2320-nm gratings are designed to reflect the fourth diffraction order into the CCD camera. The period of the bright fringe corresponds to a period of 2317 nm (of which there are four over 8-mm distance). The dim fringes repeat every 580 nm, as the fourth order has four times the accuracy of the first order. The 10- μm Moiré pattern has lower contrast. The 10- μm gratings are made using areas of five lines with a pitch of 580 nm, which are placed on a pitch of 10.000 and 10.050 μm . In this way, the 580-nm gratings diffract light into the CCD camera with a periodicity of 10.000 and 10.050 μm . The combination of 10.000 and 10.050- μm gratings results in four (low contrast) Moiré fringes over 8 mm. The high-frequency Moiré fringes result from interference of the 580-nm grating areas, which shift by 50 nm every 10 μm . Therefore, a 580-nm fringe will repeat after $580/50 \text{ nm} = 11.6$ periods of 10 μm , corresponding to 116 μm . This will result in 69 fringes over a distance of 8 mm, as is observed in Figure 14D.

The Moiré method magnifies position errors between the two gratings up to a factor of ~ 3000 . Therefore, pattern deformations are easily observed in distorted or shifted Moiré fringes. For example, the e-beam pattern generator generates stitching errors every 0.5 mm due to an inaccuracy of ~ 20 nm in the stage positioning. These errors are clearly present as discontinuities in the individual fringes of the 580-nm Moiré pattern of Figure 14D. Besides particles and pattern edge related distortions, the Moiré fringes

are straight and have a regular spacing. More importantly, the Moiré pattern is identical each time when contact with the stamp is made. From *ex-situ* laser diffraction measurements [thesis] and the *in-situ* Moiré method, we conclude that the SCIL technique is able to reproduce patterns without introducing pattern deformations that are intrinsic to the SCIL method. Particles are the principle cause of defects, but due to the elasticity of the rubber stamp, these remain localized around the particle and do not influence the pattern outside the vicinity of the particle. This confirms that the thin glass carrier provides adequate in-plane stiffness in the rubber to prevent pattern deformations.

5 SCIL overlay alignment method

Using the box-in-box alignment markers from Figure 13B, we measured stamp on substrate placement variations of $\sim 1 \mu\text{m}$. Therefore, this method is unsuitable for nanometer accurate overlay alignment. However, we found that when the stamp is kept in contact with the substrate over a small area, the stamp can be placed back in the original position to within 5 nm, as measured using the Moiré interference markers described above. This accuracy is obtained even as the stamp is released from the substrate over 9 cm from the measurement position, corresponding to an error of only 0.06 ppm. Our explanation for the remarkable accuracy is that the stamp in contact with the substrate forms a rigid connection. Furthermore, the SCIL imprint principle allows the stamp to be applied to the substrate in a stress-free manner. The reproducible stress-free application of a stamp to a substrate is possible due to Van der Waals forces that pull the PDMS stamp in contact and move the contact line forward. In effect, the SCIL method acts as a controlled stamp release mechanism. As a result, no external forces are applied to the stamp, which would deform the pattern and result in misalignment.

Figure 15 shows a schematic of the technical realization of the developed method, which is based on the highly reproducible way a stamp can be returned to a position on a substrate. The setup consists of a reference plate where the stamp is kept into contact, while the position of the chuck with respect to the reference is controlled by closed-loop piezo actuators.

The alignment method has the following sequence:

1. The stamp is in contact with reference, and contact is made with the chuck.
2. The position error between stamp and substrate is measured.

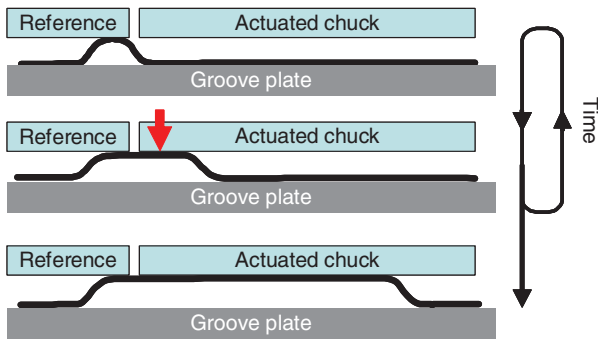


Figure 15: Method to provide overlay alignment while keeping the stamp in contact with the reference substrate. The stamp is placed in contact with the substrate held by the chuck, and the position error is measured. After retracting the stamp from the chuck, the position with respect to the reference is corrected. After making contact with the substrate, the corrected position error is measured again. Once the position is correct, the pattern is imprinted by making full contact over the substrate.

3. The stamp is released from the chuck but stays in contact with the reference.
4. The measured position error of the substrate is corrected by using the piezo actuators to position the chuck to a new position with respect to the reference.
5. The stamp is placed back into contact with the chuck, and the position is measured again.
6. →Steps 3 to 5 are repeated until the desired position of the substrate with respect to the stamp is obtained.

Once the substrate is aligned with respect to the stamp, the pattern is imprinted by fully contacting the stamp over the substrate.

5.1 SCIL imprint tool with incorporated substrate position control with nm resolution

Together with Philips Applied Technologies, a setup was designed and developed to enable the alignment method described above. The goal of the setup was to position a substrate with respect to the reference with nanometer accuracy. Figure 16A shows the schematic of the SCIL setup and an exploded view of all the components starting from the base frame (bottom), which holds the groove plate. The aluminum reference frame is composed of the quartz reference plate, aluminum chuck frame, and quartz chuck (top). Figure 16B shows a photograph of the SCIL setup consisting of the outer aluminum reference frame, which is actuated for coarse alignment by micrometer spindles. Piezo actuators and capacitive

sensors in the frame control the position of the inner black aluminum chuck frame with the quartz chuck. The reference area in Figure 15 is the quartz reference plate, which is attached to the outer aluminum base frame, see Figure 16A. The quartz reference plate is mounted in the base frame using three linear leaf springs, which compensate thermal expansion differences and keep the reference plate centered; the height of the leaf spring is ~ 20 mm to provide stiffness in the vertical direction. The reference has a square opening in the middle in which the quartz chuck fits into. The quartz chuck is placed in position in the aluminum chuck frame using metal half spheres and V-grooves at three positions; the glass is secured by pneumatic actuators. This setup allows the quartz chuck to be removed from the setup to load a substrate, while the stamp remains in contact with the reference quartz plate. The chuck frame is connected to the base frame using three elbow leaf springs. These keep the quartz chuck centered in the quartz reference and allows hysteresis-free in-plane x -, y - and rotation movement of the chuck frame for up to ~ 100 μm with low force. The height of the leaf spring is ~ 20 mm to provide stiffness in the vertical direction. Three manual vertical micrometer spindles in the base frame control the gap between the stamp and the quartz chuck/reference. On the outside of the base frame, three manual horizontal micrometer spindles can be seen, which are used to align the chuck to the stamp down to ~ 1 μm . When the quartz chuck is placed in the setup, there is between 50- and 300- μm space between the chuck and the quartz reference plate. This allows the chuck to be positioned within this range by three piezo actuators, which connect the chuck frame to the base frame. The piezo actuators have a travel range of 50 μm , and their position is controlled by capacitive sensors, operated in a closed loop. The position of the chuck frame to the base frame is measured at the three positions where the piezo is actuating the chuck. These lie on the two symmetry axes of the chuck.

The quartz chuck is required to move without hysteresis or stick-slip behavior, which means the aluminum frame may not display these phenomena as it is positioned by the piezo actuators. We therefore compared the chuck movement, given by output of the piezo capacitive sensor, with the actual movement of the chuck, which was measured using two external capacitive sensors. The external sensors are mounted on the quartz chuck and the aluminum reference frame and measure the movement between these two components. The piezo actuators are programmed to make 20 steps of 5 nm, while the positions are recorded over 60 s. The 5-nm steps are controlled by the piezo actuator's individual capacitive sensors.

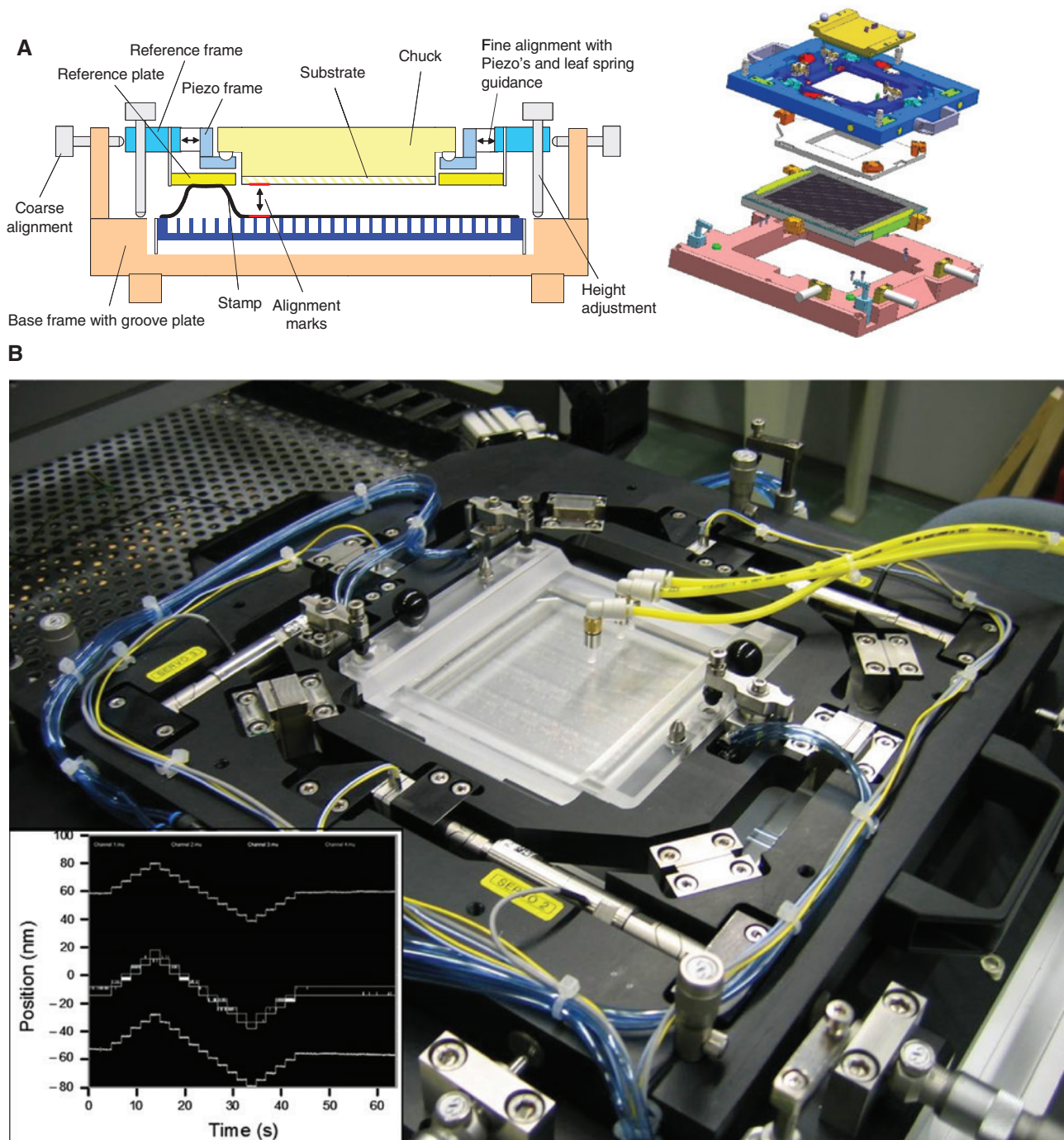


Figure 16: SCIL setup with nano-meter overlay alignment capability. (A) Schematic cross-section of the SCIL setup and exploded view of the complete assembly with from bottom to top: ground frame, groove plate, quartz reference plate, base frame, and quartz chuck. (B) Photograph of the SCIL setup with piezo feedback controlled quartz chuck. The chuck position is controlled by piezos with respect to the black aluminum frame. The distance between the two frames is measured using a capacitive sensor on the symmetry axes of the chuck where it is actuated. Inset: comparison between the position readout of external capacitive sensors (top and bottom) to the position readout of the capacitive sensors controlling the piezos when taking 5-nm steps.

The inset in Figure 16B shows position measurements as function of time as the stage is moved in 5-nm steps of the piezo's two capacitive sensors (middle) and two external capacitive sensors. As can be seen from the data,

the external sensors exactly measured the 5-nm steps. In the measurement, no stick-slip behavior is observed, and there is no hysteresis present between back and forward movements. The absolute difference between

the beginning and end position of the external sensors is caused by thermal drift in the mounts, which hold the external sensors. These measurements were performed for all three piezo's actuators and confirmed that the chuck moves reproducibly and without hysteresis over distances of $30\ \mu\text{m}$. In practice, the stamp is in contact with the quartz reference plate and not the aluminum reference frame. We compared the position of the quartz reference plate and the quartz chuck in the same manner as for the quartz chuck and the aluminum base frame. The results showed identical performance as for the measurement for the distance between the aluminum frame and quartz chuck. The high stiffness of the system allows this indirect measurement to be used and rely on the output of the piezo actuator's capacitive sensors to accurately monitor the movement of the chuck with respect to the quartz reference plate.

The alignment scheme depicted in Figure 15 can introduce an uncertainty in the position reproducibility, as the stamp has to bridge the gap between the reference plate and the substrate. This is done while the closed loop piezo system controls the position of the chuck with respect to the reference plate. We measured the reproducibility of the whole system by using the Moiré alignment markers, imprinted on a substrate, which was loaded on the quartz chuck. We found that we could reproducibly place the stamp back to within $5\ \text{nm}$ on the actively controlled substrate/chuck after it was contacted over $100\ \text{mm}$ from the reference plate to the edge of the chuck, measured the displacement using Moiré, released over $100\ \text{mm}$ back to the alignment plate, and again contacted the stamp over $100\ \text{mm}$ to measure the displacement. This demonstrates the robust overlay principle and very high accuracy of the SCIL imprint method.

5.2 Overlay alignment results

Figure 17 shows the design of the alignment markers patterns for the substrate (A) and stamp (B) used in overlay alignment experiments. The top left and right markers have box-in-box and Moiré type patterns; the top center pattern has only Moiré type markers. The left and right Moiré markers are sensitive in the y direction and used for alignment in the y direction and rotation control.

The center marker is used to align the x direction only. The distance between the two y markers is $70\ \text{mm}$, and these are located on a line $35\ \text{mm}$ above the substrate center. The stamp also contains five $2\times 2\text{-mm}$ grating areas arranged within a $3\times 3\text{-cm}$ square as indicated in Figure 17B. Within each square area, gratings with a 240-nm pitch are oriented in two perpendicular directions to enable the detection of alignment errors in two directions.

To perform overlay alignment, the position of the stamp with respect to the substrate has to be determined. This procedure is performed in a semi-automated manner using a Matlab program. First, the left and right box-in-box markers are imported simultaneously and the number of pixels between the middle cross and the surrounding box is measured in the x and y direction at four positions around the middle of the cross pattern. The width of the middle cross ($50\ \mu\text{m}$) is used to calibrate the measurement. From the measured offsets, the alignment error in the center of the substrate and the rotation error around the center are calculated. Subsequently, these values are used to calculate the piezo actuator movement to correct for the misalignment and rotation error. Using typically two to three iterations, where each time the stamp is retracted from the substrate but kept in contact with the

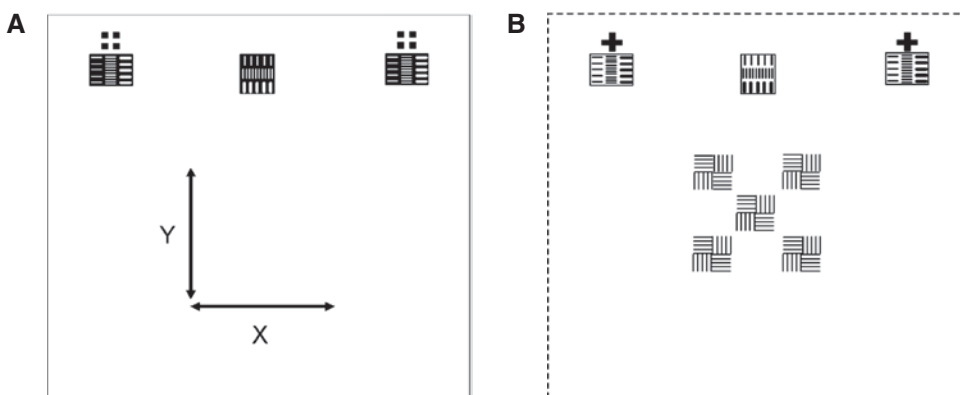


Figure 17: Schematic of the position of the alignment markers on the substrate. (A) $100\times 100\text{-mm}$ AF45 glass with imprinted alignment markers. (B) $100\times 100\text{-mm}$ area on the stamp with corresponding alignment markers and test patterns consisting of 240-nm pitch gratings in two directions.

reference, the detected offset in the center of the substrate is reduced to less than 200 nm (as calculated by the program). This corresponds to the maximum resolution of our box-in-box alignment procedure.

The box-in-box alignment ensures the pattern overlay error is less than 2 μm , which allows that the Moiré images can be used to further align the patterns. From the three alignment marker positions, Moiré patterns are imported in the Matlab program and analyzed, see Figure 18. For each Moiré pattern pair, two line scans are obtained by averaging 50 pixels in the vertical direction. For the 10- μm Moiré patterns, the high-frequency oscillations are filtered out using a Fourier transform. The resulting four fringes correspond to the 10/10.05- μm Moiré pattern and are plotted in the top right panel. Moiré patterns for the 2317/2320-nm Moiré are plotted in the bottom panel of Figure 18B without filtering. To align the patterns, two fringes are manually selected by selecting the relevant fringe peaks [see bottom panel in (B)].

From the selected data in the box, the peak is fitted using Gaussian and the peak position determined, see Figure 18C. The number of pixels between the two Gaussian peaks is determined, and the pixel size is calibrated using the known fringe spacing. This procedure is performed for the outer two Moiré markers, which gives the sample rotation and off set in y direction. From the middle marker, an offset in x direction is determined. Subsequently, in the same manner as used for the box-in-box markers, the piezo actuator movement is calculated to correct the measured misalignment. In our system, the resolution of a measured Moiré pattern is given by the number of CCD pixels per Moiré fringe. In theory, the resolution per pixel in the three different Moiré fringes is ~ 50 nm for the 10 μm , 5 nm for the 2.3 μm , and 2.5 nm for the 580-nm Moiré patterns. In practice, the alignment is

dependent on the pattern quality, which is mostly influenced by particles. This can be seen in the bottom part of Figure 18A where a particle distorts the pattern. To minimize particle-induced alignment errors, it is important to align identical fringes in subsequent imprints.

To assess the alignment performance of the whole system, we aligned the stamp containing the 240-nm gratings to the substrate. To do so, the alignment markers imprinted on the substrate are first covered with tape and then sol-gel resist is then spin coated over the substrate. After removal of the tape, the markers are free of sol-gel resist. The substrate is loaded in the SCIL setup and aligned to the stamp. This is done by only pressurizing the stamp at the alignment marker position, bringing the stamp in direct contact with the substrate at that position. After three iterations, the residuals in the offset are minimized. Next, the remainder of the substrate is contacted, thereby imprinting the gratings. To obtain contrast during later SEM inspection, the center area of the imprinted 240-nm gratings is covered with 10 nm of molybdenum using sputter deposition. Next, sol-gel resist is applied again and a second alignment is performed, after which the same grating pattern was imprinted over the first molybdenum coated layer. Both imprints have thus been separately aligned towards the alignment markers imprinted on the bare substrate.

This procedure was first performed by using the box-in-box alignment markers. Figure 19A shows a SEM image taken under an angle of 45° of the corresponding two aligned layers. As can be seen, each grating layer contains horizontally and vertically oriented grating lines. The bottom layer can be distinguished by the light color due to the molybdenum. The lines are well aligned in two directions between the first and second grating layer. The alignment error is determined by measuring

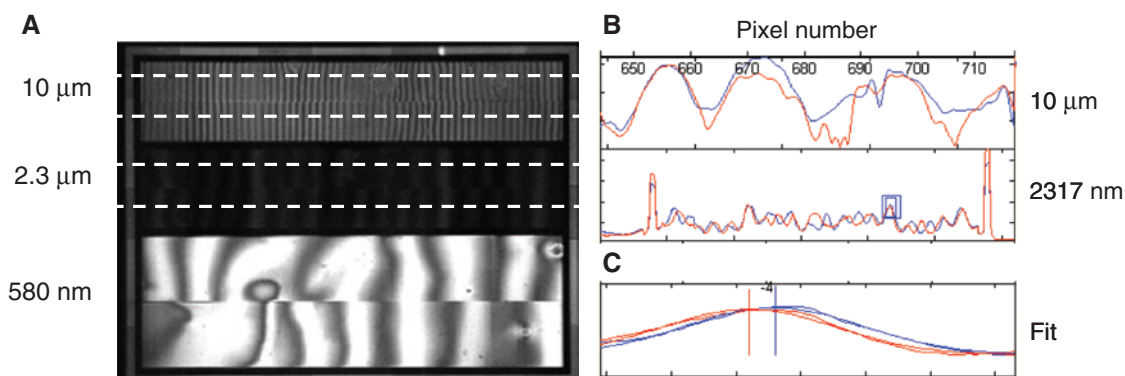


Figure 18: Moiré alignment markers in contact offset determination. (A) CCD image of Moiré interference patterns with the grating periods indicated. (B) Line scan taken through the data in (A), indicated by dashed lines. (C) Zoom in of data from 2.3- μm grating in (B) (see box) with Gaussian fit. The detected offset is 4 pixels corresponding to 20 nm.

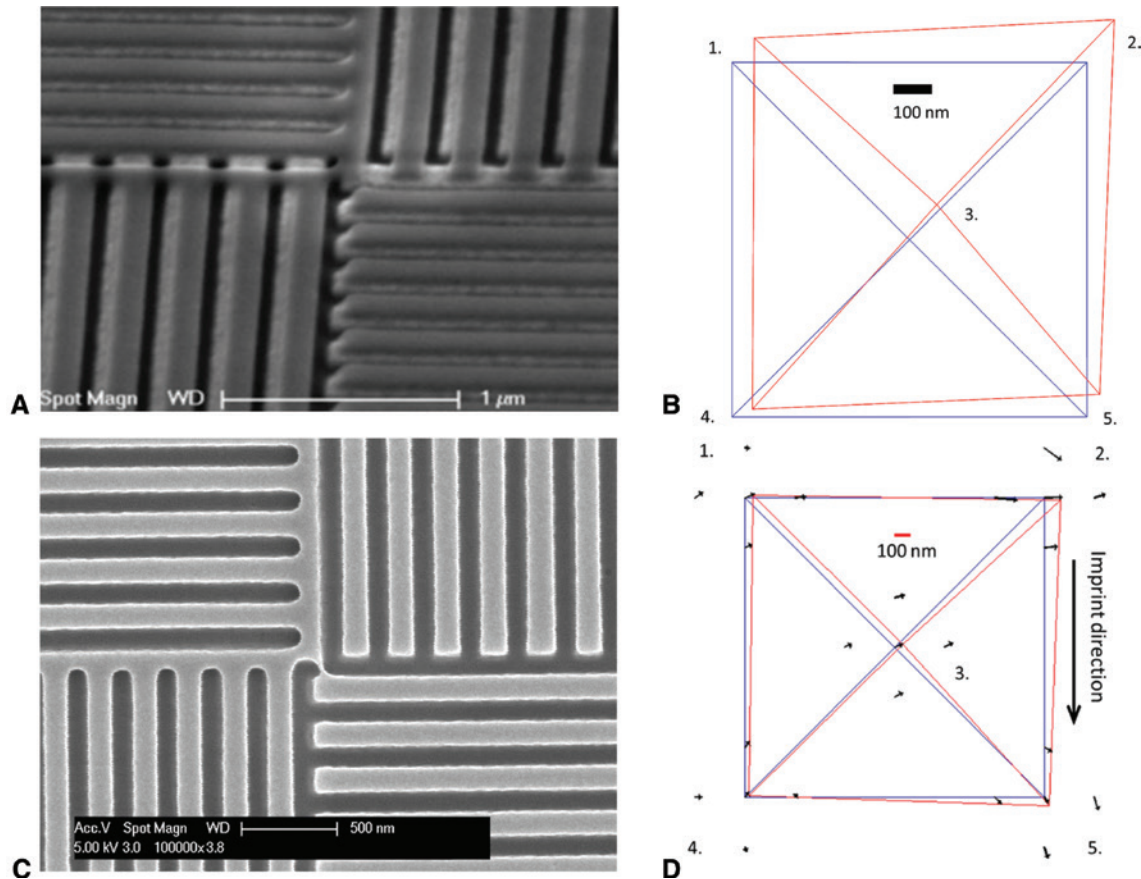


Figure 19: Determining overlay alignment for two aligned grating patterns. (A) SEM image of two aligned grating patterns in silica taken under a tilt of 45° of two aligned and imprinted gratings. (B) Schematic representation of the overlay error for five positions on the substrate using box-in-box alignment markers only. (C) SEM image of position 4 in (D), when Moiré alignment markers were used.

the offset between the first and second grating in two directions. For the image in Figure 19A, this is 21 nm in the horizontal and 55 nm in the vertical directions, respectively. Figure 19B shows an overlay error map for the five grating positions, assuming the first layer was perfectly aligned. The square corresponds to the area of the five regions, which contain gratings, see Figure 17B, and the overlay error is represented by the distance between the two squares, with the length scale indicated (100-nm scale bar). From Figure 19B, it can be seen that the maximum misalignment between the two grating layers is 110 nm (top right pattern). The maximum rotation error is found to be 1.3×10^{-6} rad. As these errors are the sum of two separate alignment runs, the alignment error for a separate run therefore is less than 55 nm. From these data, the magnification error between the first and second imprints can be calculated. We expect the error to be the result of thermal expansion variations, which are symmetric around the substrate center. Therefore, the data for the second imprint in Figure 19B are translated so that the residual overlay error is zero in the middle.

The remaining offsets for the other four points are then a measure for pattern distortion and magnification errors. We find a maximum magnification error of 1.2 ppm in the x direction and 2.4 ppm in the y direction. This is highly accurate as no active temperature control was used and there was a day between the two aligned imprints runs.

The misalignment found in Figure 19 is due to a combination of magnification errors and alignment errors. Comparing the maximum misalignment in Figure 19B of 110 nm with the magnification error over a 30×30 -mm area of 72 nm (assuming the 2.4 ppm error found above), we calculated that the maximum alignment error amounts to ~ 40 nm. Improvement in overlay accuracy can be expected as magnification errors can be eliminated by using a temperature-controlled environment during imprinting. Furthermore, the currently used alignment process only analyzes the alignment patterns and minimizes the offsets.

Figure 19C shows an SEM image of position 4, center, showing an overlay error of 22 nm in x and 14 nm in y direction. Note that the first layer has been coated with

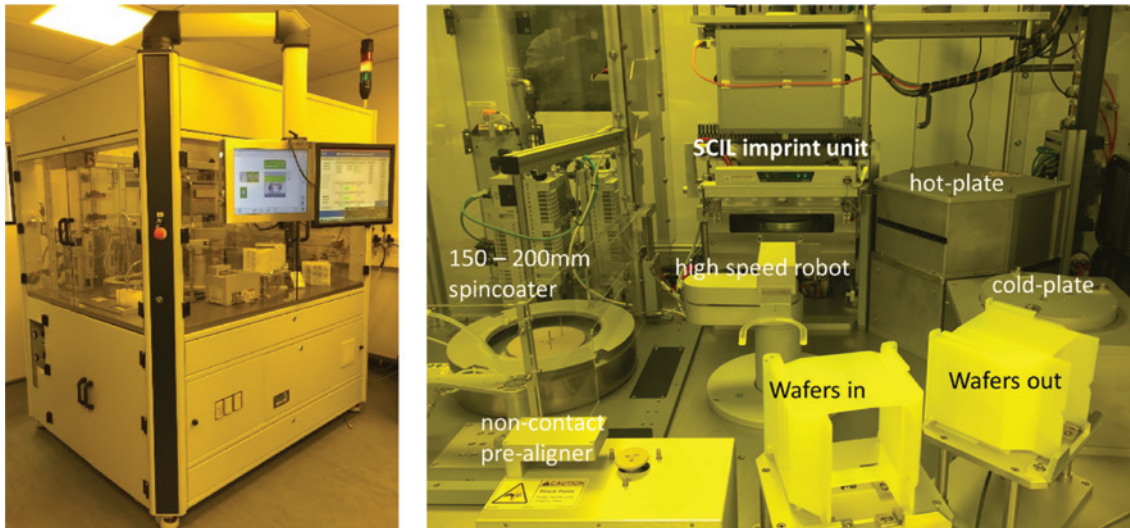


Figure 20: AutoSCIL150 high volume tool. It is built around a high speed robot with double end-effectors for increased throughput, an in- and out-put cassettes, pre-aligner, spin-coater, SCIL imprint unit, hot- and cold-plate.

10 nm over tungsten, which widens the lines by ~ 20 nm. Figure 19D shows the overlay map of 25 positions. Each position has an area of 2×2 mm², and the total area is 30×30 mm². Again in the representation, it is assumed that the first aligned and imprinted patterns are distortion-free. Calculating the alignment error for all 25 point and taking into account that it involved two separate alignment steps, we come to an alignment error of 40 nm in the x direction and 6 nm in the y direction. We attribute the relatively high error in the x direction to particles that contaminated the alignment marker and distorted the Moiré fringes. In the calculation, we did not take any magnification error corrections into account, purely the measured offset values from SEM images at 25 positions.

The high reproducibility and low pattern distortions found using the SCIL process have, to our knowledge, never been achieved by other soft imprint techniques. In fact, the reproducibility and overlay performance of soft stamp imprint techniques have only been marginally studied. A study using PDMS stamps cured against a thick glass support and Moiré pattern analysis found relative distortions of just under a micrometer over an area as small as 0.25 cm² [47]. Using the waveprint principle [46] and micro-contact printing to pattern gold on glass, an average distortion of 0.7 μ m was found over an area of 10×10 cm; a resulting overlay error up to 2 μ m was achieved over this area [32]. A recent study reported overlay errors of ~ 2.3 μ m using H-PDMS stamps and ~ 0.5 μ m when using a high modulus polymer (2600 MPa) as a stamp. These results were obtained over an area of only 50×50 μ m [20].

6 High volume manufacturing tool

Since 2008, SussMicroTec is offering an SCIL add-on module for their optical mask aligners, where an SCIL groove plate is placed at the position of the normal fused silica/chrome photo-mask. This enables up to 200-mm wafers to be automatically imprinted and released. However, the wafers must be separately coated with resist and manually loaded and unloaded from the mask aligner/SCIL tooling.

The SCIL soft nanoimprint lithography process is applicable to mass production due to the robust nature of the imprint process itself. The cluster tool developed by SCIL Nanoimprint Solutions is fully automated and allows a minimal takt time of 60 s due to the integrated aligner, spin coater, and post bake; manual handling is limited to cassette loading and unloading. Figure 20 shows pictures of the AutoSCIL tool and the individual process stations. This ensures the highest yield by eliminating contaminants introduced by handling.

In a production environment, the up-time is of high importance; furthermore, changing a stamp can potentially introduce particles in the process due to manual handling. Stamp lifetime therefore has a high priority. UV-assisted curing (sol-gel) resist systems could potentially have a higher throughput but suffer from stamp degradation [18, 19]. Although the cluster tool is equipped with a LED-UV source of 365 nm, we focus on non-UV sol-gel systems as these have demonstrated stamp lifetimes over 600 imprints. Using the cluster tool, we can accurately determine the time between spin coating the

sol-gel resist and the start of the imprint, which allows to optimize the sol-gel resist for curing behavior.

The sol-gel resist has very good adhesion to multiple substrates without the need for a primer and passes the 3M tape-test on Si, Al, Cr, sapphire, glass. Wafers are loaded in the process cassette, and the cassette is scanned for the number of loaded wafers and possible misaligned wafers and then a wafer is transferred to the centering and alignment station. After loading the aligned wafer in the spin coater, the sol-gel resist is automatically dosed and the resist spun to a uniform thickness of typically between 50 and 1000 nm. Within a defined time, the coated wafer is loaded into the SCIL imprint unit. The wafer is positioned to a gap of ~ 100 μm from the stamp after which the grooves are sequentially pressurized to ~ 20 mBar over ambient, starting from one side. Once the whole wafer has made contact, the chuck is shortly heated to 50°C to accelerate the crosslinking of the sol-gel. The chuck is cooled, and the stamp is released by sequentially switching the grooves back to vacuum, again starting from one side. Once the stamp has been released completely, the chuck is lowered and the wafer is transported to the hot plate for a post cure. This post cure can be up to 200°C , depending on the application. In general, a higher post cure leads to an increased etch resistance during dry etching in subsequent processing steps. Finally, the wafer is cooled and loaded in the wafer output cassette station. Once a wafer is processed on a station and transported to the next station, a new wafer is taken to be processed, thus after five wafers, all stations will be occupied with wafers, until the last wafer from the input cassette is taken. Currently, the imprint process is time determining and a full imprint cycle takes 90 s (wafer in to wafer out) when imprinting on silicon wafers.

The SCIL volume production tool does not include overlay alignment and is aimed at applications that require a first mask with nano-patterns. Subsequent lithography steps can align to patterns imprinted with SCIL when, in the imprint step, alignment markers are included, as is done during the VCSEL production process [22]. As was demonstrated in this paper, the SCIL method is applicable to accurate overlay alignment on wafers scale and alignment capability can be integrated in the current tooling, where the stamp and wafer can be viewed through the fused silica groove plate.

7 Conclusion

The results presented in this paper demonstrate that soft stamp based nanoimprint methods can achieve sub-10-nm resolution on wafer-scale areas. For the first time,

it was also demonstrated that flexible and soft stamps can achieve sub-10-nm overlay alignment using a table-top setup. Soft stamps have many advantages for volume production, but a key requirement is stamp lifetime, which has long been a weak point. A new inorganic, silica-based resist has demonstrated stamp lifetimes that are at least six times longer compared to what is reported in literature, without stamp degradation. Finally, the combined advantages of new materials, processes, and tooling come together in a high volume wafer-scale production tool with a throughput of up to 60 wafers per hour.

References

- [1] J. Haisma, M. Verheijen, K. Van Den Heuvel and J. Van Den Berg, *J. Vac. Sci. Technol. B* 14, 4124 (1996).
- [2] S. Y. Chou, P. R. Krauss and P. J. Renstrom, *J. Vac. Sci. Technol. B* 14, 4129 (1996).
- [3] H. Schiff, *J. Vac. Sci. Technol. B* 26, 458 (2008).
- [4] H. Gao, H. Tan, W. Zhang, K. Morton and S. Y. Chou, *Nano Lett.* 6, 2438 (2006).
- [5] J. Perumal, T. H. Yoon, H. S. Jang, J. J. Lee and D. P. Kim, *Nanotechnology* 20, 055704 (2009).
- [6] M. Okada, M. Iwasa, K.-I. Nakamatsu, K. Kanda, Y. Haruyama, et al., *Microelectronic Eng.* 86, 657 (2009).
- [7] D. Truffier-Boutry, R. Galand, A. Beaurain, A. Francone, B. Pelissier, et al., *Microelectronic Eng.* 86, 669 (2009).
- [8] D. S. Macintyre and S. Thoms, *Microelectronic Eng.* 78–79, 670 (2005).
- [9] H. Schiff, G. Kim, J. Lee and J. Gobrecht, *Nanotechnology* 20, 355301 (2009).
- [10] H. Takeishi and S. V. Sreenivasan, *Nanoimprint system development and status for high volume semiconductor manufacturing*, *Proc. of SPIE Vol. 9423*, 94230C-1 (2015).
- [11] S. Reddy and R. T. Bonnecaze, *Microelectronic Eng.* 82, 60 (2005).
- [12] D. Morihara, H. Hiroshima and Y. Hirai, *Microelectronic Eng.* 86, 684 (2009).
- [13] Y. Xia and G. M. Whitesides, *Annu. Rev. Mater. Sci.* 28, 153 (1998).
- [14] Y. Zhao, *Closely spaced polymer microstructures as a unique tool for characterization at the small scales*, *IEEE 21st International Conference on Micro Electro Mechanical Systems*, 459 (2008).
- [15] T. W. Odom, J. C. Love, D. B. Wolfe, K. E. Paul and G. M. Whitesides, *Langmuir* 18, 5314 (2002).
- [16] C. Con, J. Zhang, Z. Jahed, T. Y. Tsui, M. Yavuz, et al., *Microelectronic Eng.* 98, 246 (2012).
- [17] H. Schmitt, P. Duempelmann, R. Fader, M. Rommel, A. J. Bauer, et al., *Microelectronic Eng.* 98, 275 (2012).
- [18] M. J. Haslinger, M. A. Verschuuren, R. van Brakel, J. Danzberger, I. Bergmair, et al., *Microelectronic Eng.* 153, 66 (2016).
- [19] R. Fader, H. Schmitt, M. Rommel, A. J. Bauer, L. Frey, et al., *Microelectronic Eng.* 98, 238 (2012).
- [20] J. A. Rogers, K. E. Paul and G. M. Whitesides, *J. Vac. Sci. Technol. B* 16, 88 (1998).

- [21] S. Pagliara, L. Persano, A. Camposeo, R. Cingolani and D. Pisignano, *Nanotechnology* 18, 175302 (2007).
- [22] M. A. Verschuuren, P. Gerlach, H. A. van Sprang and A. Polman, *Nanotechnology* 22, 505201 (2011).
- [23] J. J. Wierer, A. David and M. M. Megens, *Nat. Photonics* 3, 163 (2009).
- [24] M. Verschuuren and H. van Sprang, *Mater. Res. Soc. Sym. Proc.* 1002, N03 (2007).
- [25] Z. Geng, X. Guo, Q. Kan and H. Chen, *AIP Adv.* 5, 041308 (2015).
- [26] X. Wang, A. Albrecht, H. H. Mai, C. Woigt, T. Meinl, et al., *Micro Electronic Eng.* 110, 44 (2013).
- [27] P. Spinelli, M. A. Verschuuren and A. Polman, *Nat. Commun.* 3, 692 (2012).
- [28] V. E. Ferry, M. A. Verschuuren, M. C. Lare, R. E. I. Schropp, H. A. Atwater, et al., *Nano Letters* 11, 4239 (2011).
- [29] G. Lozano, D. J. Louwers, S. R. K. Rodriguez, S. Murai, O. T. A. Jansen, et al., *Light Sci. Applications* 2, e66 (2013).
- [30] G. Lozano, G. Grzela, M. A. Verschuuren, M. Ramezani and J. Gomez Rivas, *Nanoscale* 6, 9223 (2014).
- [31] M. A. Verschuuren, M. J. A. de Dood, D. Stolwijk, G. W. 't Hooft and A. Polman, *MRS Commun.* 5, 547 (2015).
- [32] A. Pierret, M. Hocevar, S. L. Diedenhofen, R. E. Algra, E. Vlieg, et al., *Nanotechnology* 21, 065305 (2010).
- [33] S. L. Diedenhofen, O. T. A. Janssen, M. Hocevar, A. Pierret, E. P. A. M. Bakkers, et al., *ACS Nano* 5, 583 (2011).
- [34] E. Östman, U. B. Arnalds, E. Melander, V. Kapaklis, G. K. Pálsson, et al., *New J. Phys.* 16, 053002 (2014).
- [35] U. B. Arnalds, J. Chico, H. Stopfel, V. Kapaklis, O. Bärenbold, et al., *New J. Phys.* 18, 023008 (2016).
- [36] F. Hua, A. Gaur, Y. Sun, M. Word, N. Jin, et al., *IEEE Trans. Nanotechnol.* 5, 301 (2006).
- [37] M. A. Verschuuren, *Substrate Conformal Imprint Lithography for Nanophotonics*, PhD. Thesis, Utrecht University, 2010.
- [38] M. M. J. Decré, R. Schneider, D. Burdinski, J. Schellekens, M. Saalmink, et al., *Mater. Res. Soc. Symp. Proc.* M4.9.1 (2004).
- [39] J. Schellekens, D. Burdinski, M. Saalmink, M. Beenhakkers, G. Gelinck, et al., *Mater. Res. Soc. Symp. Proc.* M2.9.1 (2004).
- [40] M. Forthner, M. Rumler, F. Stumpf, R. Fader, M. Rommel, et al., *Appl. Phys. A* 122, 240 (2016).
- [41] R. Fader, *Substratkonforme Imprintlithographie/öptische Anwendungen*, PhD. Thesis, Friedrich-Alexander-Universität Erlangen-Nürnberg, 2014.
- [42] P. C. Duineveld, M. Lilja, T. Johansson and O. Inganäs, *Langmuir* 18, 9554 (2002).
- [43] T. Balla, S. M. Spearing and A. Monk, *J. Phys. D Appl. Phys.* 41, 174001 (2008).
- [44] R. Fader, M. Förthner, M. Rumler, M. Rommel, A. J. Bauer, et al., *Structure placement accuracy of wafer level stamps for substrate conformal imprint lithography*, NNT 2014, 13th International Conference on Nanoimprint and Nanoprint Technology, Kyoto, Japan, 2014.
- [45] R. Fader, M. Rommel, A. Bauer, M. Rumler, L. Frey, et al., *J. Vac. Sci. Technol. B* 31, 06FB02 (2013).
- [46] M. Mühlberger, I. Bergmair, W. Schwinger, M. Gmainer, R. Schöftner, et al., *Microelectronic Eng.* 84, 925 (2007).
- [47] L. Chen, X. Deng, J. Wang, K. Takahashi and F. Liud, *J. Vac. Sci. Technol. B* 23, 2933 (2005).

**Marc A. Verschuuren**

Philips SCIL Nanoimprint Solutions,
De Lismortel 31, 5612 AR, Eindhoven,
The Netherlands
marc.verschuuren@philips.com

Marc A. Verschuuren received a bachelor degree in Chemical Engineering from the Fontys University, Eindhoven, The Netherlands in 2002. In 2010 he obtained his PhD on Substrate Conformal Imprint Lithography for nanophotonics from the Utrecht University, The Netherlands, supervised by Prof. Albert Polman from the AMOLF institute. Marc worked at Philips research Eindhoven, The Netherlands as senior scientist and project leader from 2001–2015 on various projects such as printable LCD backplanes, micro-patterning for garment care, micro-structured transparent ceramics, 3D photonic crystals, 2D photonic crystals for LEDs, VCSEL lasers, nano-LEDs and plasmonics for: photovoltaics and general LED illumination. All the applications required large area nano- and micro-patterning and during this time he developed the nanoimprint method Substrate Conformal Imprint Lithography. Since 2015 he started the Philips venture SCIL Nanoimprint solutions, developing SCIL based volume production solutions.

**Mischa Megens**

Philips Research, High Tech Campus 4,
5656AE, Eindhoven, The Netherlands

**Yongfeng Ni**

Philips Research, High Tech Campus 4,
5656AE, Eindhoven, The Netherlands

Yongfeng Ni received the B.Eng. degree in Optical Engineering from Zhejiang University, Hangzhou, China, in 1997. He was research assistant at Zhejiang University from 1997 to 2001 and was research assistant at Central Research Laboratory of Hamamatsu Photonics, Japan from 1998 to 1999. He carried out his doctoral research at FOM institute AMOLF, Amsterdam from 2001 to 2005 and received the PhD degree in laser physics from Radboud University Nijmegen, the Netherlands in 2006. He was with Philips Research Laboratory, Eindhoven, the Netherlands from 2006 to 2010. Since 2011, he has been with ASML, Veldhoven, the Netherlands, currently working on EUV illumination, imaging simulation and wafer alignment.

**Hans van Sprang**

Philips Research, High Tech Campus 4,
5656AE, Eindhoven, The Netherlands

Hans van Sprang has studied Chemistry and Physics at Leyden university and started to work at Philips Research in 1980. He worked on various topics like Liquid Crystal Display physics, analytical X-ray instrumentation and analysis and optical materials for Lighting applications. In this context he was first project leader of the work on SCIL and later on hosted the project in the Photonic Materials and Devices Department which he headed from 2008 till 2015.

**Albert Polman**

AMOLF, Amsterdam, The Netherlands

Albert Polman is scientific group leader and program leader at the AMOLF Institute in Amsterdam, the Netherlands. He is associated with the University of Amsterdam as a professor of Photonic materials for photovoltaics. Polman's research focuses on nanophotonics: the control, understanding and application of light at the nanoscale, with special emphasis on light management in solar cells and optical metamaterials. In parallel, his group has developed angle-resolved cathodoluminescence spectroscopy as a new tool for super-resolution imaging. Polman obtained his PhD from the University of Utrecht, was post-doctoral researcher at AT&T Bell Laboratories and then became group leader at AMOLF, where he also served as director from 2006–2013. He has published over 300 papers in photonics and photovoltaics.